Lawrence Berkeley National Laboratory

Title

Changes in Reactivity as Chemistry Becomes Confined to an Interface. The Case of Free Radical Oxidation of C30H62 Alkane by OH

Permalink

https://escholarship.org/uc/item/8s96t5pq

Journal

The Journal of Physical Chemistry Letters, 9(5)

ISSN

1948-7185

Authors

Houle, Frances A
Wiegel, Aaron A
Wilson, Kevin R

Publication Date

2018-03-01

DOI

10.1021/acs.jpclett.8b00172

Peer reviewed

Changes in reactivity as chemistry becomes confined

1

to an interface. The case of free radical oxidation of

2

$C_{30}H_{62}$ alkane by OH

3

4   *Frances A. Houle,* Aaron A. Wiegel and Kevin R. Wilson**

5   Chemical Sciences Division, Lawrence Berkeley National Laboratory, 1 Cyclotron Road,

6   Berkeley, CA 94720

7 Corresponding Authors: fahoule@lbl.gov, krwilson@lbl.gov
8
9

10

11ABSTRACT

12Here we examine in a simple organic aerosol the transition between heterogeneous chemistry

13under well-mixed conditions to chemistry under interfacial confinement. A single reaction

14mechanism, shown to reproduce observed OH oxidation chemistry for liquid and semisolid

15$C_{30}H_{62}$, is used in reaction-diffusion simulations to explore reactivity over a broad viscosity

16range. The results show that when internal mixing of the aerosol is fast and the particle interface

17is enriched in C-H groups, ketone and alcohol products, formed via peroxy radical

18disproportionation, predominate. As viscosity increases the reactions become confined to a shell

19at the gas-aerosol interface. The confinement is accompanied by emergence of acyloxy reaction

20pathways that are particularly active when the shell is 1nm or less. We quantify this trend using

21a reaction-diffusion index, allowing the parts of the mechanism that control reactivity as

22viscosity increases to be identified.

23

24TOC graphic

25

26
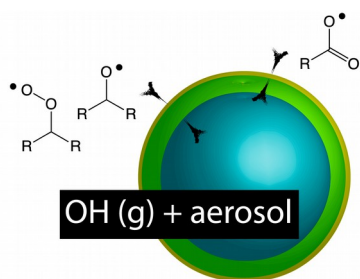
INTRODUCTION

28

29   The presence of aerosols in the troposphere increases substantially the complexity of

30models for the chemical evolution of planetary atmospheres. This complexity is due in large part

31to chemistry that couples gas and condensed phase reaction mechanisms. Aerosol reactivity with

32a gas is generally measured with an uptake coefficient, γ, which is calculated from composition

33data using the expression

34          $$\gamma = \frac{2 k_{rx} d_p \rho_0 N_A}{3 cM} \quad (1)$$

35where k_{rx} is the apparent disappearance rate constant for the starting material in the aerosol, d_p is

36the particle diameter, ρ_0 is the aerosol density, c is the velocity of the gaseous reactant molecules,

37M is the molecular weight of the aerosol material, and N_A is Avogadro's number. This expression

38applies if the aerosol is well mixed and the entire volume of the particle participates in the

39reaction. However, the rates of multiphase processes such as heterogeneous reactions[1-7] and

40evaporation[8-11] and condensation kinetics are inextricably connected to internal mixing timescales

41in aerosols. These timescales can span many orders of magnitude and are controlled by water

42content and aerosol phase state (liquid, solids and glasses).

43   Discovery of predictive elementary reaction mechanisms that take diffusion into account

44provides some insights to how transport affects reactivity. For example, Knopf *et al.*[2] and Davies

45*et al.*,[3] observed a complex nonlinear relationship between the organic diffusion constant and OH

46reaction rate (i.e. effective reactive uptake) with levoglucosan and citric acid aerosol,

47respectively. Berkemeier et al.,[12] used a kinetic multilayer model to explain the complex time

48 dynamics of O_3 uptake onto glassy and semi-solid shikimic acid. This complex relationship was

49 used to identify more broadly how a multiphase system can evolve through limiting kinetic

50 regimes represented by trajectories through a "kinetic cube".[13]   Houle *et al.*,[4] showed how the

51 uptake coefficient depends upon both the timescales for a reactive surface collision and internal

52 mixing, showing that multiphase uptake should be considered an emergent property of the

53 system (gas + particle), rather than a measure of the intrinsic reactivity of the interface. This

54 description is consistent with results reported by Wiegel *et al.*,[5] who showed that for OH

55 reactions with semisolid alkane aerosols, there is no straightforward relationship between

56 measurements of an effective uptake coefficient obtained in experiment and the inherent OH

57 reactivity of triacontane.

58   These previous studies elucidate how diffusion affects consumption kinetics for specific

59 cases. Here we consider broader trends, looking at how reactivity (i.e. product distribution)

60 evolves with changes in the internal aerosol mixing times when the governing reaction

61 mechanism is held constant. Our approach is to examine $C_{30}H_{62}$ aerosol + OH, whose mechanism

62 has been validated for liquid and semi-solid phases,[5, 14] and systematically vary the alkane

63 diffusion coefficient (viscosity) in between these extrema to trace how the free radical chain and

64 product distributions depend on viscosity. We connect reactivity to diffusion by defining a

65 reaction-diffusion index that quantifies the governing kinetics, and links them to specific sections

66 of the reaction mechanism.

67 **RESULTS AND DISCUSSION**

68

69   A   reaction-diffusion model framework for OH + $C_{30}H_{62}$ alkane aerosol has been

70 constructed from known chemistry and rate coefficients, and validated using experimental data

71 for liquid $C_{30}H_{62}$, squalane,[4, 14] and its semisolid isomer, triacontane.[5] A diagram of the reaction

72 mechanism is presented in Scheme S1 in the Supplementary Information. The free radical chain

73 reaction is initiated by H abstraction from a C-H bond located near the surface of the particle.[4-5,]

74 [14-15] The resulting alkyl radical reacts rapidly with O_2 to form a peroxy radical. Peroxy radicals

75 disproportionate to form mainly alcohols and ketones in C-H rich environments via the Russell

76 and/or Bennet-Summers mechanisms, but also have minor channels forming alkoxy and acyloxy

77 radicals that lead to aldehyde and carboxylic functionalities, as well as fragmentation to form

78 new alkyl radicals.[5, 14] This chemistry is not represented explicitly in the simulations, rather, the

79 alkane is treated as a collection of functional groups and carbon backbones that track formation

80 of free radical intermediates (such as peroxy and acyloxy radicals), stable product functional

81 groups (such as ketones), and backbone fragments (such as C_{24}). This description allows the free

82 radical chemistry to be represented across the entire oxidation process, from a pure alkane to

83 complete conversion into CO_2, using a tractable number of reaction steps.

84   In this work, we focus on trends in reactivity that would be observed in a typical flow

85 tube experiment using the reaction scheme for triacontane, which is the same as for squalane but

86 does not have tertiary alkyl functionalities. Flow tubes are often used to provide data on aerosol

87 reactions that can be used for atmospheric chemistry models. Reaction-diffusion simulations

88 have been performed using a gas phase OH density of 5.04 x 10^{10} molec/cm^3 [16, 17] and the reaction

89 time 60s, which are typical conditions for flow tube measurements. Liquid squalane has a self-

90 diffusion coefficient of 8.5 x 10^{-7} cm^2/s,[18] and is well-mixed. Test simulations revealed that this

91 behavior persists until a value of 1 x 10^{-11} cm^2/s, therefore we restricted the $C_{30}H_{62}$ diffusion

92 coefficients D to the range from 1 x 10^{-11} - 8.39 × 10^{-19} cm^2/s (the self-diffusion coefficient of

93 triacontane[5]). All product species in the simulation are assumed to diffuse with the same

94 coefficient as the alkane. Viscosity changes may occur as a result of oxidation.[5, 19] These effects

95 are neglected in the present work in order to focus on broad trends. To provide a unified way to

96 characterize reactivity across such a broad range of diffusion coefficients, we define a reaction-

97 diffusion index (I_{RD}). I_{RD} is a dimensionless number calculated from timescales, and is similar to

98 the Damköhler number, or the square of the Thiele modulus;[20]

99
$$I_{RD} = k_{rx}[gas] \tau_{cd} \qquad (2)$$

100 where k_{rx} is a phenomenological rate constant for consumption of starting material, as used in (1),

101 and τ_{cd} is the characteristic complete mixing time for a particle of a specific diameter.[6] The

102 reaction-diffusion index can be written for the specific $C_{30}H_{62}$ viscosities (D), OH density

103 ([OH(g)]) and particle size:

104 $$I_{RD} = \frac{k_{rx}[OH(g)]d_p^2}{4\pi^2 D} (3)$$

105 If $I_{RD} \ll 1$, mixing is fast relative to arrival of OH at the aerosol surface and the supply

106 of OH is rate limiting. If $I_{RD} \gg 1$, the rate of mixing to bring organic molecules to the aerosol

107 surface is rate limiting. If $I_{RD} = 1$, then reaction rates and internal transport rates are balanced.

108 This is the midpoint of the transition between kinetically limiting regimes.

109 Figure 1 shows the initial uptake coefficients, γ, calculated from simulated $C_{30}H_{62}$

110 disappearance curves as a function of D and I_{RD}: they undergo a significant decrease in the range

111 $D = 10^{-12}$ - 10^{-14} cm^2/s. This sigmoidal dependence of γ on D is consistent with previous

112 experimental observations in levglucosan and citric acid as well as with predictions of Houle et

113al.[4] The free radical reactions initiated by OH uptake generate oxygen-containing functionalities

114(ketones, alcohols, aldehydes, carboxylic acids); their predicted fractions in the particle at 60s are

115shown in Figure 2. When I_{RD} is small, *i.e.* the OH radical supply is rate limiting and the alkane is

116liquid, ketones and alcohols are the primary products as found previously in simulations of

117squalane oxidation.[14] As D decreases, I_{RD} is large and mixing is rate limiting, and ketones become

118the dominant functional group accompanied by a modest increase in carboxylic acids and

119disappearance of aldehydes and alcohols. The full time-dependent product compositions and
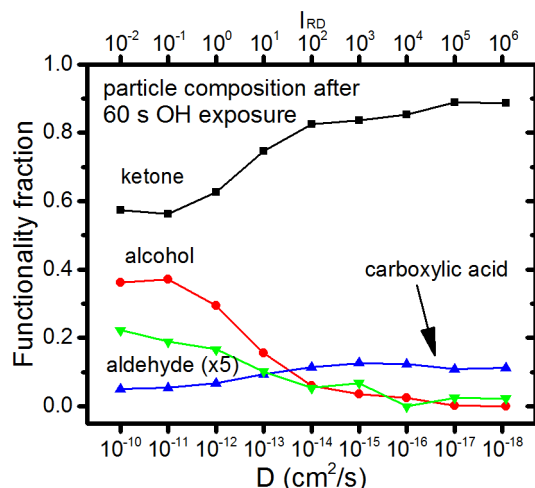
120maps
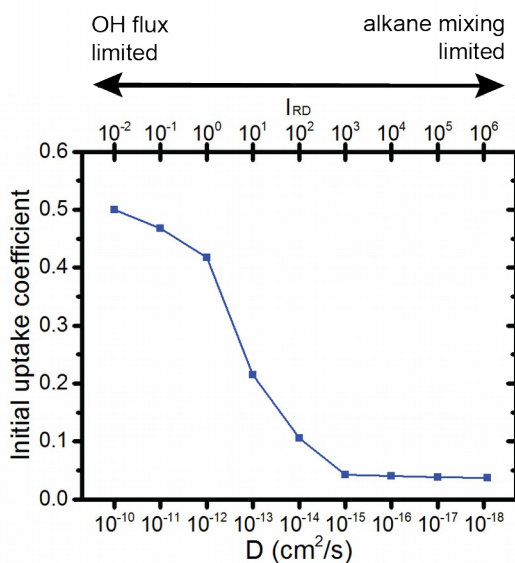
121

122**Figure 1**. Initial uptake coefficient calculated from $C_{30}H_{62}$ disappearance curves as a function of

123diffusion coefficient and I_{RD}.

124.

125

126

Figure 2. Product functionality fractions in the aerosol as a function of diffusion coefficient and I_{RD}.

of unreacted $C_{30}H_{62}$ within the particle are shown in Figure S1 in the Supplementary Information.

It is evident that the decrease in γ and change in product distributions is accompanied by a transition from chemistry under well-mixed conditions to chemistry under confinement to the near-surface region of the aerosol.

The extent of confinement for a particular D has been described in terms of a reacto-diffusion length, L. It is the thickness of a shell that is accessible for chemistry surrounding the particle core. L is given by

$$L = \left(\frac{8\,D}{[gas]\,c\pi\,\sigma d_p^2} \right)^{1/2} (4)$$

where [*gas*] is the density of the gaseous reactant, and σ is the probability that a colliding gas molecule will stick to the aerosol surface long enough to react.[4] In the limit of complete mixing on the timescale of the chemistry, $d_p = 2L$, and a more general form of (1) is

$$140 \quad \gamma = \frac{2 k_{rx} \rho_0 N_A}{3 c M d_p^2} \left[d_p^3 - (d_p - 2L)^3 \right] \quad (5)$$

141   Equations (4) and (5) predict that γ decreases as D and L decrease. Equation (4) also

142 assumes that k_{rx} is constant under all conditions, i.e. the reactivity does not change. A value for

143 k_{rx} applicable to a particular I_{RD}, [OH(g)] and D can be estimated from (5). For $I_{RD} = 1$, a 200 nm

144 diameter particle under flow tube conditions and $D = 1 \times 10^{-12}$ cm^2/s, $k_{rx} = 2.12 \times 10^{12}$ molecules

145 cm^{-3} s. This is essentially the same as the phenomenological rate constant for the initial decay of

146 $C_{30}H_{62}$ when the aerosol is well-mixed (2.16×10^{12} molecules cm^{-3} s).[15] When $D > 1 \times 10^{-12}$ cm^2/s

147 and $I_{RD} < 1$, the aerosol particle is reasonably well-mixed (Figure S1), and reaction is controlled

148 by the arrival and reaction of OH at the aerosol surface. When $D < 1 \times 10^{-12}$ cm^2/s and $I_{RD} > 1$, the

149 reaction is controlled by the rate of internal mixing of the aerosol at a particular value of D, *i.e.*

150 delivery of unreacted C-H bonds to the surface. As I_{RD} is varied from 10^{-2} to 10^{6}, corresponding

151 to the range of D used in the present calculations, k_{rx} varies about $\pm 6\%$ (see Table S1 and Figure

152 S2 in the SI). This variation in rate coefficient is modest, and could be interpreted to mean that

153 the chemical reaction does not change much over this very broad range in diffusivities. Such a

154 conclusion is not consistent with the dramatic change in product distributions shown in Figures 2

155 and S1, however.

156   It is evident from equations (1), (3) and (5) that γ, L and I_{RD} are related. Substituting (3)

157 into (4),

$$158 \quad L = \left(\frac{2 k_{rx}}{I_{RD} \pi^3 c \sigma} \right)^{1/2} \quad (6)$$

159 This relationship allows the reaction-diffusion length to be connected to the balance between

160 reaction and diffusion to be assessed over the entire range of conditions linking the limiting

161 cases.

162   What does this tell us about trends in product formation? Figures 2 and S1 show that

163 disproportionation chemistry to form ketones and alcohols is favored when the reactions are

164 limited by OH – particle collisions ($I_{RD} < 0.1$). As the reactions become mixing limited ($I_{RD} > 10$)

165 and diffusively confined to the interface, ketones are the major component of the particle

166 because alcohols and aldehydes are consumed by abstraction by OH and by reaction with

167 additional peroxy radicals that are formed by fragmentation during the free radical chain reaction

168 (see Scheme S1). Further insights are possible using marker species in the simulations, which is

169 straightforward using the stochastic simulation methodology, to determine the nature of

170 reactivity as I_{RD} varies. Abstraction markers track the number of OH abstraction events, which

171 occur predominately at the surface of the aerosol and initiate the free radical chain reaction.[4, 21]

172 Disproportionation markers track the number of bimolecular reaction events involving peroxy

173 radicals of all types. Fragmentation is the major chain propagation process. C_{30} fragmentation

174 markers track dissociation of the initial $C_{30}H_{62}$ alkane backbone at random locations via alkoxy

175 radical formation and decomposition, which leads to formation of volatile fragments and mass

176 loss from the particle. Acyloxy radical fragmentation markers track CO_2 loss from the end of the

177 oxidized alkane, an "unzipping" process that becomes important when the aerosol has become

178 heavily oxidized.[5]

179
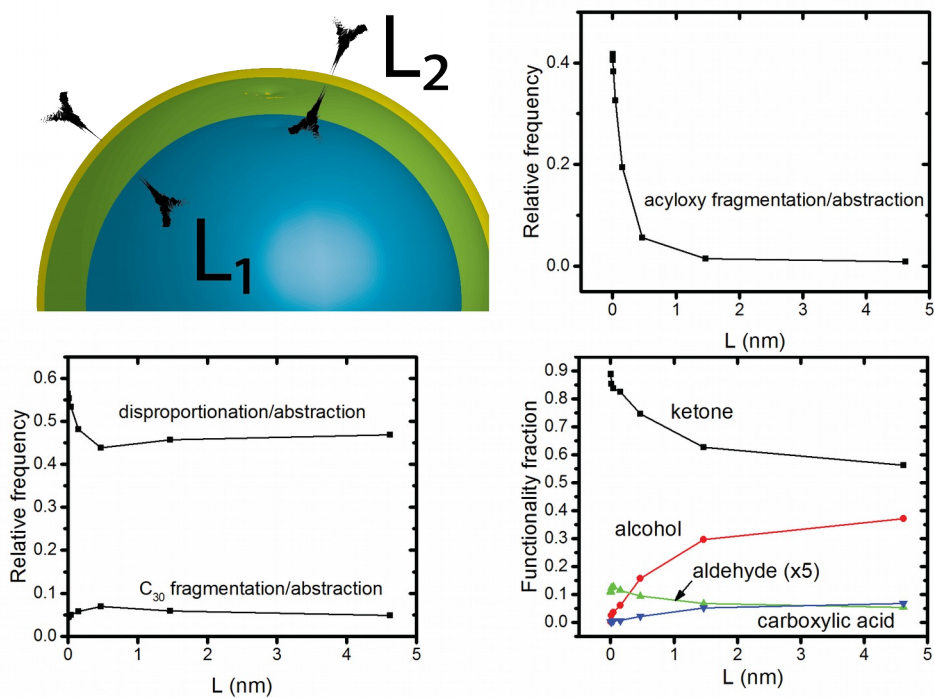
181 **Figure 3**. Frequency of disproportionation and fragmentation and acyloxy radical fragmentation

182 reactions, and fraction of each functionality formed during the oxidation reaction, as a function of

183 the reacto-diffusion length L. The reaction frequencies are calculated by normalizing the number

184 of events of each type to the number of abstraction events. The range for L corresponds to $10^{-1} \leq$

185 $I_{RD} \leq 10^2$, and 10^{-14} cm^2/s $\leq D \leq 10^{-11}$ cm^2/s. Disproportionation and fragmentation occur

186 essentially uniformly over this range, denoted as L_1. Acyloxy fragmentation has a much smaller

187 characteristic reacto-diffusion length, L_2, and leads to a significant change in functionalities

188 formed.

189

190   By normalizing disproportionation, C$_{30}$ fragmentation and acyloxy fragmentation to OH

191 abstraction events for each value of D and using Equation (6), we can establish a measure of the

192 relative importance of each of these parts of the free radical chain reaction as a function of the

11   11

193reacto-diffusion length L as shown in Figure 3. Disproportionation and C_{30} fragmentation both

194involve reactions that are second order in peroxy radical concentration, and have a characteristic

195L_I that extends up to the center of the particle when viscosity is low.[5, 14] Acyloxy fragmentation,

196on the other hand, is very different. The unimolecular "unzipping" reaction is only kinetically

197significant at a much smaller L_2 (< 1nm), and the oxidation process is confined to the outer

198surface of the aerosol. This indicates that as the reaction-diffusion length for a system changes,

199not only does the average composition of the particle change, the dominant part of the reaction

200mechanism also changes. This result shows that it cannot be assumed that measurements of γ

201trends and k_{rx} for a particular system are easily connected to the chemical reactions of a particular

202aerosol across a range of conditions.

203   Finally, the simulations show that measurements of composition at the exit of the flow

204tube are meaningful as snapshots, but cannot be assumed to reveal the dominant chemistry. As

205seen in Figure S1, at the earliest times for all D and I_{RD}, ketone and alcohol functionalities are

206produced at the same rate, but then diverge. This indicates that while C-H bonds are abundant,

207the Russell mechanism for disproportionation is operative. As C-H bonds become constrained,

208ketones become the dominant product functionality at all times. This represents a transition from

209disproportionation chemistry to functionalization + fragmentation chemistry. The extent of this

210transition is clearly time-dependent as well as D-dependent, indicating that there is no clear

211steady-state regime for the reaction under flow tube conditions.

212

213**CONCLUSIONS**

214

215   Detailed simulations such as those presented here are essential to connect observations to

216 fundamental reactivity. We show evidence that internal mixing times in organic aerosols have a

217 substantial effect on the product distributions, going well beyond simple considerations of rates

218 under limiting regimes. We have used I_{RD} to connect quantitatively trends in reactivity with

219 diffusion coefficient D to reacto-diffusion lengths L using a single chemical mechanism. The

220 results show that specific elementary reaction pathways (within a network of possible elementary

221 steps) have characteristic L and can become dominant under certain transport conditions, leading

222 to substantial and nonlinear changes in overall aerosol chemistry with changes in diffusion. This

223 means that measurements of uptake coefficients and extraction of effective rate constants for

224 various classes of chemicals are challenging to use directly to predict the oxidative evolution of

225 average aerosol properties such as size, average carbon oxidation state, optical and cloud

226 nucleation properties in very different environments such as the atmosphere. Construction of

227 detailed models such as that reported here provides an effective tool for identifying dominant

228 factors controlling reactivity and creating realistic models for aerosol reactions in the

229 troposphere.

230

231 **METHODS**

232

233   All simulations were performed using Kinetiscope, a stochastic chemical kinetics

234 simulation software package.[22] The initial aerosol diameter is chosen to be 200 nm, and is

235 represented in the simulation by a stack of 200 13.17 nm × 13.17 nm × 0.5 nm compartments

236 along the radius spanning the center to the outer surface of the particle. The compartment

237volumes are allowed to vary according to product densities and the extent of gas product

238volatilization in order to maintain accurate concentrations.

239

250

251**SUPPORTING INFORMATION.** Reaction scheme for free radical reactions in alkanes

252initiated by OH reactions. Particle compositions as a function of time. Table of reactivity metrics

253for each simulation. Plot of apparent rate constants. This material is available free of charge via

254the Internet at http://pubs.acs.org.

255

256 REFERENCES

1. Arangio, A. M.; Slade, J. H.; Berkemeier, T.; Pöschl, U.; Knopf, D. A.; Shiraiwa, M., Multiphase Chemical Kinetics of Oh Radical Uptake by Molecular Organic Markers of Biomass Burning Aerosols: Humidity and Temperature Dependence, Surface Reaction, and Bulk Diffusion. *The Journal of Physical Chemistry A* **2015**, *119*, 4533-4544.

2. Slade, J. H.; Knopf, D. A., Multiphase Oh Oxidation Kinetics of Organic Aerosol: The Role of Particle Phase State and Relative Humidity. *Geophysical Research Letters* **2014**, *41*, 5297-5306.

3. Davies, J. F.; Wilson, K. R., Nanoscale Interfacial Gradients Formed by the Reactive Uptake of Oh Radicals onto Viscous Aerosol Surfaces. *Chem. Sci.* **2015**, *6*, 7020-7027.

4. Houle, F. A.; Hinsberg, W. D.; Wilson, K. R., Oxidation of a Model Alkane Aerosol by Oh Radical: The Emergent Nature of Reactive Uptake. *Phys. Chem. Chem. Phys.* **2015**, *17*, 4412-4423.

5. Wiegel, A. A.; Liu, M.; Hinsberg, W. D.; Wilson, K. R.; Houle, F. A., Diffusive Confinement of Free Radical Intermediates in the Oh Radical Oxidation of Semisolid Aerosol. *Physical Chemistry Chemical Physics* **2017**, *19*, 6814-6830.

6. Shiraiwa, M.; Ammann, M.; Koop, T.; Pöschl, U., Gas Uptake and Chemical Aging of Semisolid Organic Aerosol Particles. *Proceedings of the National Academy of Sciences of the United States of America* **2011**, *108*, 11003-8.

7. Shiraiwa, M.; Zuend, A.; Bertram, A. K.; Seinfeld, J. H., Gas-Particle Partitioning of Atmospheric Aerosols: Interplay of Physical State, Non-Ideal Mixing and Morphology. *Physical chemistry chemical physics : PCCP* **2013**, *15*, 11441-53.

8. Zhang, H.; Worton, D. R.; Shen, S.; Nah, T.; Isaacman-VanWertz, G.; Wilson, K. R.; Goldstein, A. H., Fundamental Time Scales Governing Organic Aerosol Multiphase Partitioning and Oxidative Aging. *Environmental Science & Technology* **2015**, *49*, 9768-9777.

9. Saleh, R.; Donahue, N. M.; Robinson, A. L., Time Scales for Gas-Particle Partitioning Equilibration of Secondary Organic Aerosol Formed from Alpha-Pinene Ozonolysis. *Environmental Science & Technology* **2013**, *47*, 5588-5594.

10. Vaden, T. D.; Imre, D.; Beránek, J.; Shrivastava, M.; Zelenyuk, A., Evaporation Kinetics and Phase of Laboratory and Ambient Secondary Organic Aerosol. *Proceedings of the National Academy of Sciences of the United States of America* **2011**, *108*, 2190-2195.

11. Ingram, S.; Cai, C.; Song, Y.-C.; Glowacki, D. R.; Topping, D. O.; O'Meara, S.; Reid, J. P., Characterising the Evaporation Kinetics of Water and Semi-Volatile Organic Compounds from Viscous Multicomponent Organic Aerosol Particles. *Physical Chemistry Chemical Physics* **2017**, *19*, 31634-31646.

12. Berkemeier, T.; Steimer, S. S.; Krieger, U. K.; Peter, T.; Poschl, U.; Ammann, M.; Shiraiwa, M., Ozone Uptake on Glassy, Semi-Solid and Liquid Organic Matter and the Role of Reactive Oxygen Intermediates in Atmospheric Aerosol Chemistry. *Physical Chemistry Chemical Physics* **2016**, *18*, 12662-12674.

13. Berkemeier, T.; Huisman, A. J.; Ammann, M.; Shiraiwa, M.; Koop, T.; Pöschl, U., Kinetic Regimes and Limiting Cases of Gas Uptake and Heterogeneous Reactions in

297 Atmospheric Aerosols and Clouds: A General Classification Scheme. *Atmos. Chem. Phys.* **2013**,
298 *13*, 6663-6686.

299 14.　　Wiegel, A. A.; Wilson, K. R.; Hinsberg, W. D.; Houle, F. A., Stochastic Methods for
300 Aerosol Chemistry: A Compact Molecular Description of Functionalization and Fragmentation
301 in the Heterogeneous Oxidation of Squalane Aerosol by Oh Radicals. *Phys. Chem. Chem. Phys.*
302 **2015**, *17*, 4398-4411.

303 15.　　Smith, J. D.; Kroll, J. H.; Cappa, C. D.; Che, D. L.; Liu, C. L.; Ahmed, M.; Leone, S. R.;
304 Worsnop, D. R.; Wilson, K. R., The Heterogeneous Reaction of Hydroxyl Radicals with Sub-
305 Micron Squalane Particles: A Model System for Understanding the Oxidative Aging of Ambient
306 Aerosols. *Atmos Chem Phys* **2009**, *9*, 3209-3222.

307 16.　　Lambe, A. T., et al., Characterization of Aerosol Photooxidation Flow Reactors:
308 Heterogeneous Oxidation, Secondary Organic Aerosol Formation and Cloud Condensation
309 Nuclei Activity Measurements. *Atmos Meas Tech* **2011**, *4*, 445-461.

310 17.　　Kang, E.; Root, M. J.; Toohey, D. W.; Brune, W. H., Introducing the Concept of
311 Potential Aerosol Mass (Pam). *Atmos Chem Phys* **2007**, *7*, 5727-5744.

312 18.　　von Meerwall, E.; Beckman, S.; Jang, J.; Mattice, W. L., Diffusion of Liquid N-Alkanes:
313 Free-Volume and Density Effects. *J Chem Phys* **1998**, *108*, 4299-4304.

314 19.　　Song, Y. C.; Haddrell, A. E.; Bzdek, B. R.; Reid, J. P.; Barman, T.; Topping, D. O.;
315 Percival, C.; Cai, C., Measurements and Predictions of Binary Component Aerosol Particle
316 Viscosity. *J Phys Chem A* **2016**, *120*, 8123-8137.

317 20.　　Levenspiel, O., Chemical Reaction Engineering. *Ind Eng Chem Res* **1999**, *38*, 4140-4143.

318 21.　　Lee, L.; Wilson, K., The Reactive–Diffusive Length of Oh and Ozone in Model Organic
319 Aerosols. *The Journal of Physical Chemistry A* **2016**, *120*, 6800-6812.

320 22.　　Hinsberg, W. D.; Houle, F. A. Kinetiscope: (Http://Hinsberg.Net/Kinetiscope/.

321